Intensity Effects on Inverse-Bremsstrahlung Electron Acceleration

R. Pakter

Plasma Science and Fusion Center

Massachusetts Institute of Technology

Cambridge, Massachusetts 02139

Abstract

The effects of beam intensity on the laser field on Inverse-Bremsstrahlung Electron Acceleration are investigated. A self-consistent Hamiltonian formalism that takes into account both particles and wave dynamics is developed. It is shown that efficient acceleration is achieved for high-density beams. However, for such high densities, beam plasma effects impose a limitation on energy gain. A method is proposed in order to remove the limiting effects.

41.75.Ht

With the advent of powerful coherent radiation-generation systems a good deal of effort has been directed to the analysis of new concepts for particle acceleration that can overcome the acceleration gradient limitations of current linear accelerators [1]. Among different methods proposed for laser-particle acceleration a promising branch is the one where particles and electromagnetic fields interact directly without the aid of dielectrics or plasmas [2–7], because of the difficulties to control instabilities and other damaging effects generated by the presence of such media. In particular, Kawatana and co-workers introduced the concept of Inverse-Bremsstrahlung Electron Acceleration [5], where a *small* electrostatic field applied perpendicular to a propagating electromagnetic wave breaks the symmetry in the oscillatory wave-particle interaction. They showed that with properly chosen values for the applied electrostatic field strength, net energy gain is obtained in one cycle of the wave. By analyzing the nonlinear equations involved in the single-particle-wave interaction, Hussein and Pato [6] demonstrated that by alternating the direction of the applied electrostatic field at appropriate positions, the acceleration is extended for more than one wave cycle, leading to high energy gain. They called this scheme as Nonlinear Amplification of Inverse-Bremsstrahlung Electron Acceleration (NAIBEA). Subsequent analysis on the wave-particle interaction based on particle-in-cell simulations indicated that although space-charge forces are negligible, beam current effects on the electromagnetic fields may play an important role in the acceleration process [8].

In this paper we further investigate beam current effects in the NAIBEA scheme. A self-consistent Hamiltonian formalism that takes into account both particles and wave dynamics is developed. It is shown that, if on one hand, increasing densities are necessary in order to achieve efficient acceleration, on the other hand, it causes beam plasma effects to become pronounced, setting certain limits on the energy gain. A method is proposed to overcome these limitations.

We consider a beam of electrons of charge $-e$ and mass m interacting with an applied plane electromagnetic wave propagating in the x-direction and an applied electrostatic field pointing along the y-direction. The vector potential that describes the electromagnetic wave

is written as

$$\frac{e\mathbf{A}}{mc^2} = -\frac{1}{2}\mathcal{A}\, e^{i\varphi}\, \hat{\mathbf{e}}_y + c.c., \tag{1}$$

where c is the speed of light *in vacuo*, $\varphi \equiv \omega t - kx$, with ω being the wave frequency and $k = \omega/c$ the wave number, $\mathcal{A}$ is the complex wave amplitude, and *c.c.* stands for complex conjugate. The wave electric and magnetic fields are then given by $\mathbf{E}_{wave} = E_y \hat{\mathbf{e}}_y$ and $\mathbf{B}_{wave} = B_z \hat{\mathbf{e}}_z$, with $E_y = B_z = i\,\mathcal{E}\, e^{i\varphi}/2 + c.c.$ and $\mathcal{E} = mc\omega\mathcal{A}/e$. Normalizing space to $1/k$, time to $1/\omega$, energy to mc^2, momentum to mc, vector potential to e/mc^2 and electric field to $e/mc\omega$, the dynamics of the i^{th} electron in the beam is described by the following particle Hamiltonian

$$H_i = \gamma_i + E_{app} y_i, \tag{2}$$

where

$$\gamma_i = \{1 + P_{xi}^2 + [P_{yi} + A_y]^2 + P_{zi}^2\}^{1/2} \tag{3}$$

is the relativistic mass factor, $\mathbf{P}_i = \mathbf{p}_i - \mathbf{A}$ is the canonical momentum, with $\mathbf{p}_i$ being the mechanical momentum, and E_{app} is the normalized applied electrostatic field in the y-direction. The energy equation for the particle is readily obtained from Eq. (2) as

$$\dot{H}_i = -v_{yi} E_y, \tag{4}$$

where the dot stands for derivative with respect to t and $\mathbf{v}_i = \mathbf{p}_i/\gamma_i$ is the normalized (to c) particle velocity. The NAIBEA scheme consists of alternating the sign of a properly chosen E_{app} at the positions where the phase φ satisfies $\varphi = (2n+1)\pi/2$, $n = 1, 2, \cdots$. With this alternation, one shows that the right-hand-side of Eq. (4) is always positive leading to continuous particle energization [6].

To self-consistently take into account the effects generated by beam current on the electromagnetic fields we apply a formalism which is similar to that employed in Ref. [9]. We start from Maxwell equation for the vector potential (in normalized form)

$$\left(\frac{\partial^2}{\partial x^2} - \frac{\partial^2}{\partial t^2}\right) A_y = -\frac{4\pi e^2 k}{mc^2} J_y, \tag{5}$$

where

$$J_y = -\sum_{i=1}^{N} v_{yi}(t)\, \delta[\mathbf{r} - \mathbf{r}_i(t)] \tag{6}$$

is the y-component of the electron current density, which has been normalized to eck^3. Here, N is the total number of particles in the system, and $\mathbf{r}_i(t)$ is the instantaneous displacement of the i^{th} particle. From Eq. (5) one readily derives a slow-time scale evolution equation for the complex wave amplitude as

$$\dot{\mathcal{A}} = \frac{4\pi i e^2 k}{mc^2 VT} \int J_y\, e^{-i(t'-x')} d^3r' dt', \tag{7}$$

where a Fourier transform over the fast (primed) variables has been performed introducing the volume V and period T. Using the polar representation for the wave amplitude $\mathcal{A} = \sqrt{\rho}\, e^{i\sigma}$, Eq. (6), and the relation

$$v_{yi}(t') = \frac{P_{yi} + A_y[x_i(t'), t']}{\gamma_i} \tag{8}$$

we can re-write Eq. (7) in the form

$$\dot{\sigma} = -\frac{\delta}{\sqrt{\rho} N} \sum_{i=1}^{N} \frac{[P_{yi} - \sqrt{\rho}\cos(t - x_i + \sigma)]}{\gamma_i} \cos(t - x_i + \sigma), \tag{9}$$

$$\dot{\rho} = -\frac{2\delta\sqrt{\rho}}{N} \sum_{i=1}^{N} \frac{[P_{yi} - \sqrt{\rho}\cos(t - x_i + \sigma)]}{\gamma_i} \sin(t - x_i + \sigma), \tag{10}$$

where use has been made of the conditions $v_{xi} \approx 1$ and $|\dot{P}_{yi}| = |E_{app}| \ll 1$. The effect of the electron current density on the electromagnetic fields appears through the parameter

$$\delta \equiv \omega_b^2/\omega^2, \tag{11}$$

where $\omega_b^2 = 4\pi e^2 n_e/m$ is the beam plasma frequency squared, with n_e being the average electron density.

An interesting point is that rescaling the wave dynamical quantities according to $\sigma = 2\bar{\sigma}/N$ and $\rho = \delta\bar{\rho}$ one concludes that all relevant dynamical equations for both particles and fields can be derived from one generalized Hamiltonian given by

$$\mathcal{H} = \sum_{i=1}^{N} H_i = \sum_{i=1}^{N} [\gamma_i + E_{app} y_i], \tag{12}$$

$$\gamma_i = \{1 + P_{xi}^2 + [P_{yi} - \sqrt{\delta\bar{\rho}}\cos(t - x_i + 2\bar{\sigma}/N)]^2 + P_{zi}^2\}^{1/2}. \tag{13}$$

In the above Hamiltonian formalism the equations of motion for the particles and the wave quantities are given, respectively, by

$$\begin{aligned} \dot{x}_i &= \partial\mathcal{H}/\partial P_{xi}, \qquad \dot{y}_i = \partial\mathcal{H}/\partial P_{yi}, \qquad \dot{z}_i = \partial\mathcal{H}/\partial P_{zi}, \\ \dot{P}_{xi} &= -\partial\mathcal{H}/\partial x_i, \quad \dot{P}_{yi} = -\partial\mathcal{H}/\partial y_i, \qquad \dot{P}_{zi} = 0, \end{aligned} \tag{14}$$

and

$$\dot{\bar{\sigma}} = \frac{\partial\mathcal{H}}{\partial\bar{\rho}}, \;\; \dot{\bar{\rho}} = -\frac{\partial\mathcal{H}}{\partial\bar{\sigma}}, \tag{15}$$

where $\bar{\sigma}$ and $\bar{\rho}$ play the role of canonically conjugated coordinate and momentum, respectively.

It readily follows from the generalized Hamiltonian in Eq. (12) that the energy exchange between particles and electromagnetic wave obeys a conservation law of the form [10]

$$\frac{N\bar{\rho}}{2} + \sum_{i=1}^{N}(\gamma_i + E_{app} y_i) = \text{const.} \tag{16}$$

Note that $mc^2(N\bar{\rho}/2) = u_{wave} V_d$ is the total electromagnetic energy stored in the wave, where $u_{wave} = |\mathcal{E}|^2/8\pi$ is the wave energy density and $V_d = V/k^3$ is the dimensional volume.

In order to analyze the self-consistent interaction in a NAIBEA scheme, we numerically integrate the set of equations (14) and (15). We model the interaction considering a cold beam of N electrons per wavelength of the laser field, homogeneously distributed along the x-direction. We consider a specific example discussed in previous papers [6,11], namely, a 10 μm wavelength laser with electric field amplitude $|\mathcal{E}| = 1.636 \times 10^9$ V/cm, which corresponds to an intensity of 3.5×10^{15} W/cm^2. The strength of the applied electrostatic

field is $|E_{app}| = 4.28 \times 10^{-5}|\mathcal{E}|$. The electrons are injected with an energy corresponding to $\gamma = 106.8$ at an angle of 0.608° with respect to the x-axis. For this case, the single-particle (not self-consistent) analysis, based on Eq. (2), reveals that an electron initially at $x(0) = 0$ attain a final energy corresponding to $\gamma = 850$ after 96 cm of interaction when one inversion in the sign of E_{app} is performed. The optimal position for the electrostatic field reversion (i.e., when $\varphi = 3\pi/2$) is found to be 32.8 cm from the injection point.

Now we investigate what happens when the wave dynamics is taken into account. We consider two distinct cases, a low-density beam with $\delta = 5 \times 10^{-8}$ and a high-density beam with $\delta = 10^{-3}$. We note that although the values of δ are different from those found in Ref. [11], they correspond to equivalent beam densities since the normalization adopted there introduces a factor of $2\pi/32 \approx 0.2$ in the definition of δ {compare Eq. (20) in [11] with Eq. (11) in this paper}. In Fig. 1 we show the results obtained for the self-consistent interaction with $N = 50$ particles per wavelength when one inversion in E_{app} is performed at the optimal position determined by the single-particle analysis. The number of particles in the simulation is chosen to obtain convergent (independent of N) results for the wave dynamical quantities. To compare self-consistent results with single-particle results, one particle is chosen among the N particles as a *tag* particle whose energy is monitored during the acceleration. The *tag* particle is launched exactly with $x(0) = 0$ (which is the initial condition used in the single-particle analysis). The figure presents the amplitude (a) and phase (b) of the wave, and the energy (in terms of γ) of the *tag* particle (c) as a function of the dimensional interaction distance $s = x/k$ for both the low-density case (dashed curves) and the high-density case (solid curves).

For the low-density case with $\delta = 5 \times 10^{-8}$ (dashed curves) the wave is essentially unaffected by the presence of particles, with $\bar{\rho}$ and $\bar{\sigma}$ keeping their values unchanged throughout the interaction, as seen in Figs. 1(a) and 1(b). Hence, the acceleration shown in Fig. 1(c) agrees with that found in the single-particle analysis where a maximum energy corresponding to $\gamma = 850$ is attained at $s = 96.0$ cm. Despite the large particle energization, it should be pointed out that the acceleration process for low densities is clearly *inefficient*, since little

energy is transferred from the wave to the particle beam.

For the high-density case with $\delta = 10^{-3}$ (solid curves), however, the acceleration process is dramatically affected by the wave dynamics. Figure 1(a) shows that the wave is severely damped as it interacts with the particle beam, transferring up to 70% of its initial energy to the beam. As a result of wave depletion, the instantaneous rate of energy change given by Eq. (4) is reduced, and the maximum energy obtained by the *tag* particle is decreased to $\gamma = 350$ [see Fig. 1(c)]. Although the final energy in the high-density case is much lower than that in the low-density case, it still represents a good acceleration with gradients on the order of hundreds of MeV/m.

By examining the high-density case in more detail, one readily finds another reason for the limited particle acceleration, besides the wave depletion. Figure 1(b) shows that beam plasma effects cause the wave phase velocity to increase, which is indicated by a nearly monotonic increase in $\bar{\sigma}$. Because phase synchronous is required in the NAIBEA scheme, even small changes in $\bar{\sigma}$ can drive particles and wave out of phase, eventually changing the sign of $-v_{yi}E_y$ in Eq. (4) and ceasing the acceleration process.

To overcome the limitation on particle acceleration imposed by the beam-plasma-induced phase shift, we notice, from the generalized Hamiltonian in Eq. (12), that the effective wave phase seen by the particles is $\varphi_{sc} = \varphi + 2\bar{\sigma}/N$ instead of φ. Thus, by changing the sign of E_{app} according to $\varphi_{sc} = (2n+1)\pi/2$, $n = 1, 2, \cdots$, we can compensate self-consistent variations of the wave phase, thereby prolonging the acceleration process.

To test the efficacy of the compensation procedure, we consider the high-density beam example presented in Fig. 1. Integrating the self-consistent set of equations (14) and (15), we readily obtain the interaction distance s for which $\varphi_{sc} = 3\pi/2$ is satisfied: $s = 28.0$ cm. In Fig. 2, the wave amplitude $\bar{\rho}$ (solid curve) and the *tag* particle energy γ (dashed curve) are shown as a function of s for the case where E_{app} is changed at the optimized position $s = 28.0$ cm. Comparing these results with the previous results in Figs. 1(a) and 1(c), solid curves, one observes apparent improvements in the acceleration process with a 20% increase in the total energy delivered by the wave to the particle beam, as well as a 30%

increase in the energy attained by the *tag* particle. To better analyze the overall efficiency of high-density beam acceleration, we also perform a simulation with the same parameters used in Fig. 2, using a larger number of particles: $N = 1000$. The particle energy distribution function $f(\gamma)$ obtained for $s = 67.8$ cm is presented in Fig. 3. Although beam heating takes place, the fact that 20% of the particles are accelerated beyond $\gamma = 400$ demonstrates the efficacy of the acceleration scheme.

To place above results into certain perspective, two remarks are in order. First, although the results in this paper are obtained for the particular laser particle acceleration scheme, i.e., Inverse-Bremsstrahlung Electron Acceleration, one might expect that similar effects may occur in other laser accelerator schemes. Second, the formalism developed here may be generalized to describe a phased array of laser beams interacting with an electron beam in a NAIBEA scheme, which was proposed in ref. [11] in order to avoid the laser diffraction problem.

In conclusion, we have investigated the effects of beam intensity on the laser field on the NAIBEA scheme. In particular, a self-consistent Hamiltonian formalism that takes into account both particles and wave dynamics has been developed. It was found that high particle gain and efficient energy exchange between wave and particles can be achieved simultaneously for high-density beams if beam plasma effects are judiciously taken into account.

ACKNOWLEDGMENTS

The author thanks Dr. C. Chen for valuable discussions and a careful reading of the manuscript. This work was supported by CAPES, Brazil and in part by U.S. Department of Energy under grant No. DE-FG02-95ER-40919.

REFERENCES

[1] *Advanced Accelerator Concepts*, edited by P. Schoessow, AIP Conf. Proc. No. 335 (AIP, New York, 1995).

[2] P. K. Kaw and R. M. Kulsrud, Phys. Fluids **16**, 321 (1973).

[3] D. J. Larson, Phys. Rev. Lett. **71**, 851 (1993).

[4] B. Hafizi, A. Ting, E. Esarey, P. Sprangle, and J. Krall, Phys. Rev. E **55**, 5924 (1997).

[5] S. Kawatana, T. Maruyama, H. Watanabe, and I. Takahoshi, Phys. Rev. Lett. **66**, 2072 (1991).

[6] M. S. Hussein and M. P. Pato, Phys. Rev. Lett. **68**, 1136 (1992).

[7] M. S. Hussein, M. P. Pato, and A. K. Kerman, Phys. Rev. A **46**, 3562 (1992).

[8] A. C. J. Paes, M. Virgínia Alves, R. M. O. Galvão, A. Serbeto, and M. S. Hussein, J. Plasma Phys. **57**, 697 (1997).

[9] R. Pakter, R. S. Schneider, and F. B. Rizzato, Phys. Rev. E **49**, 1594 (1994).

[10] The energy conservation law is obtained by applying a canonical transformation to the generalized Hamiltonian in Eq. (12) given by the generating function $F_2(\bar{\sigma}, \bar{\rho}'; t) = (t + 2\bar{\sigma}/N)\bar{\rho}'$ (prime here refers to transformed variables), which leads to $\bar{\sigma}' = t + 2\bar{\sigma}/N$ and $\bar{\rho}' = N\bar{\rho}/2$. The transformed Hamiltonian $\mathcal{H}' = \mathcal{H} + N\bar{\rho}/2$ is now a constant of motion since it does not depend explicitly on time. The constancy of $\mathcal{H}'$ readily leads to the energy conservation in Eq. (16).

[11] R. M. O. Galvão, M. S. Hussein, M. P. Pato, and A. Serbeto, Phys. Rev. E **49**, R4807 (1994).

FIGURES

FIG. 1. Amplitude (a) and phase (b) of the wave, and energy of the *tag* particle (c) as a function of the interaction distance s, for $\delta = 5 \times 10^{-8}$ (dashed curves) and $\delta = 10^{-3}$ (solid curves). Here, one inversion in E_{app} is performed at the position determined by the single-particle analysis $s = 32.8$ cm. The laser is a 10 μm wavelength with an initial amplitude $|\mathcal{E}| = 1.636 \times 10^9$ V/cm, and the applied electric field is given by $|E_{app}| = 4.28 \times 10^{-5}|\mathcal{E}|$. The simulations are performed with $N = 50$ particles per wavelength.

FIG. 2. Wave amplitude and *tag* particle energy as a function of the interaction distance s for the high-density case $\delta = 10^{-3}$ when the inversion in E_{app} is performed at the optimized position $s = 28.0$ cm. Remaining parameters are the same as in Fig. 1.

FIG. 3. Energy distribution function $f(\gamma)$ obtained for $s = 67.8$ cm and $N = 1000$ particles per wavelength when the inversion in E_{app} is performed at the optimized position $s = 28.0$ cm. Remaining parameters are the same as in Fig. 2.

Fig. 1

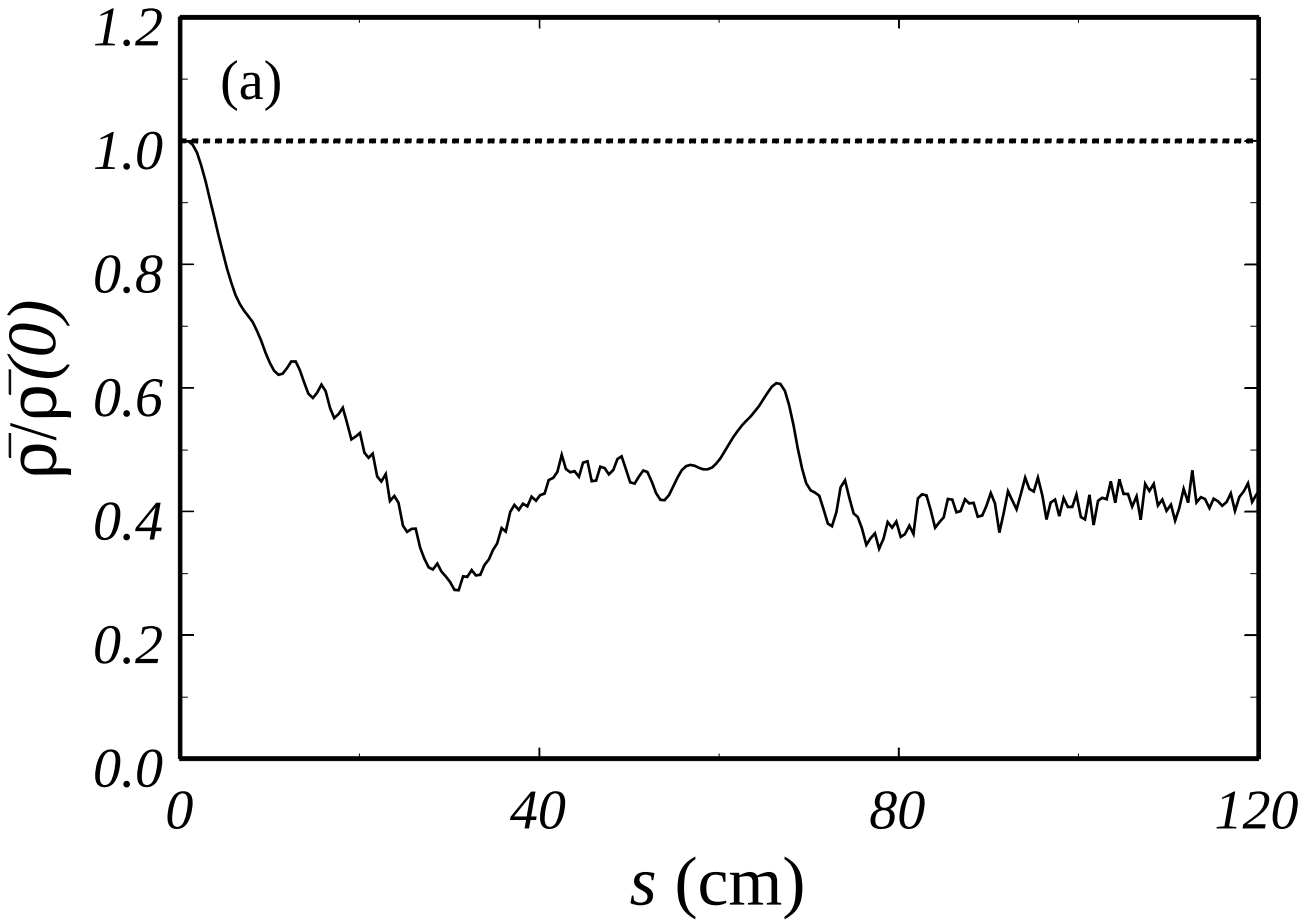

Fig. 1

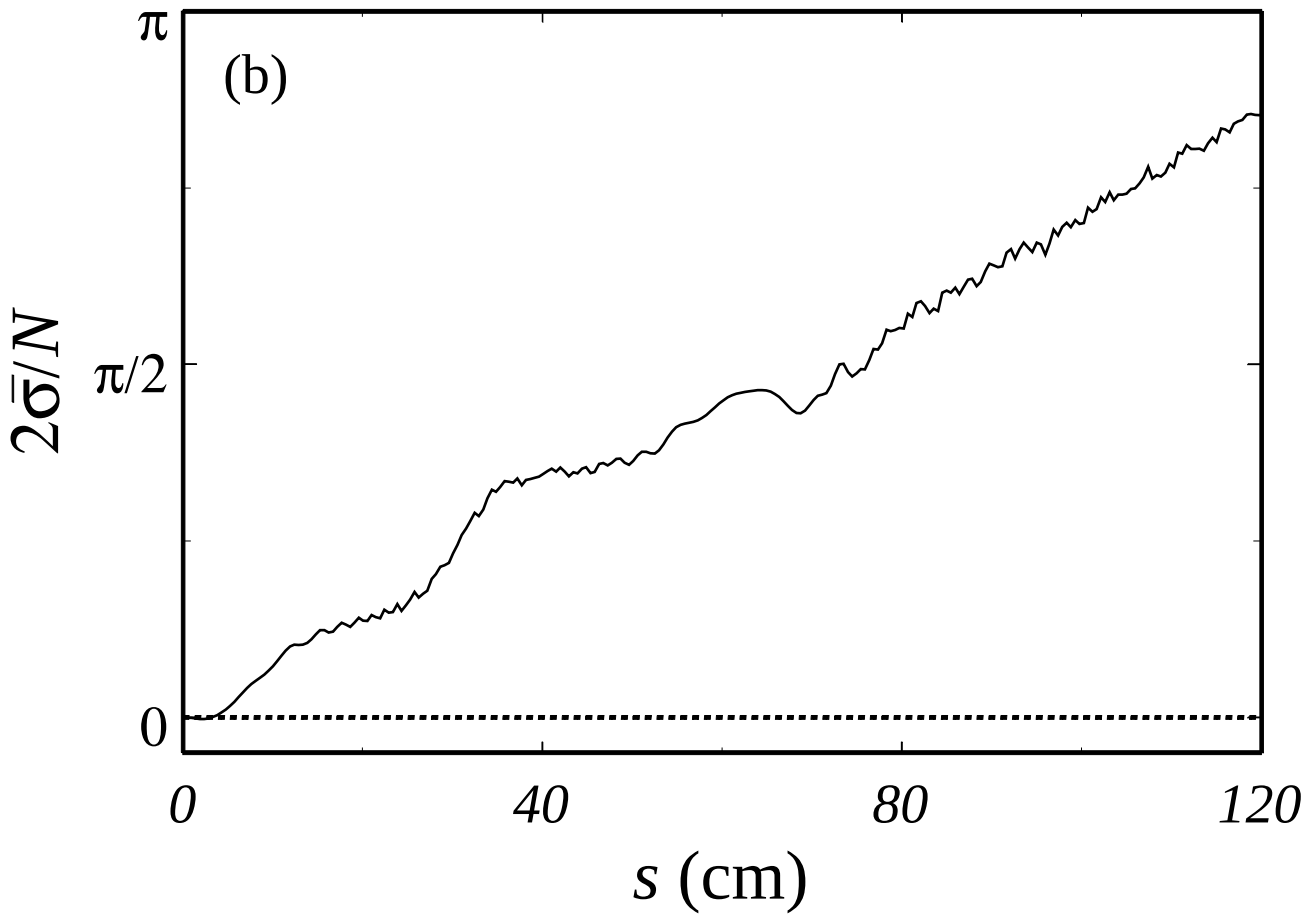

Fig. 1

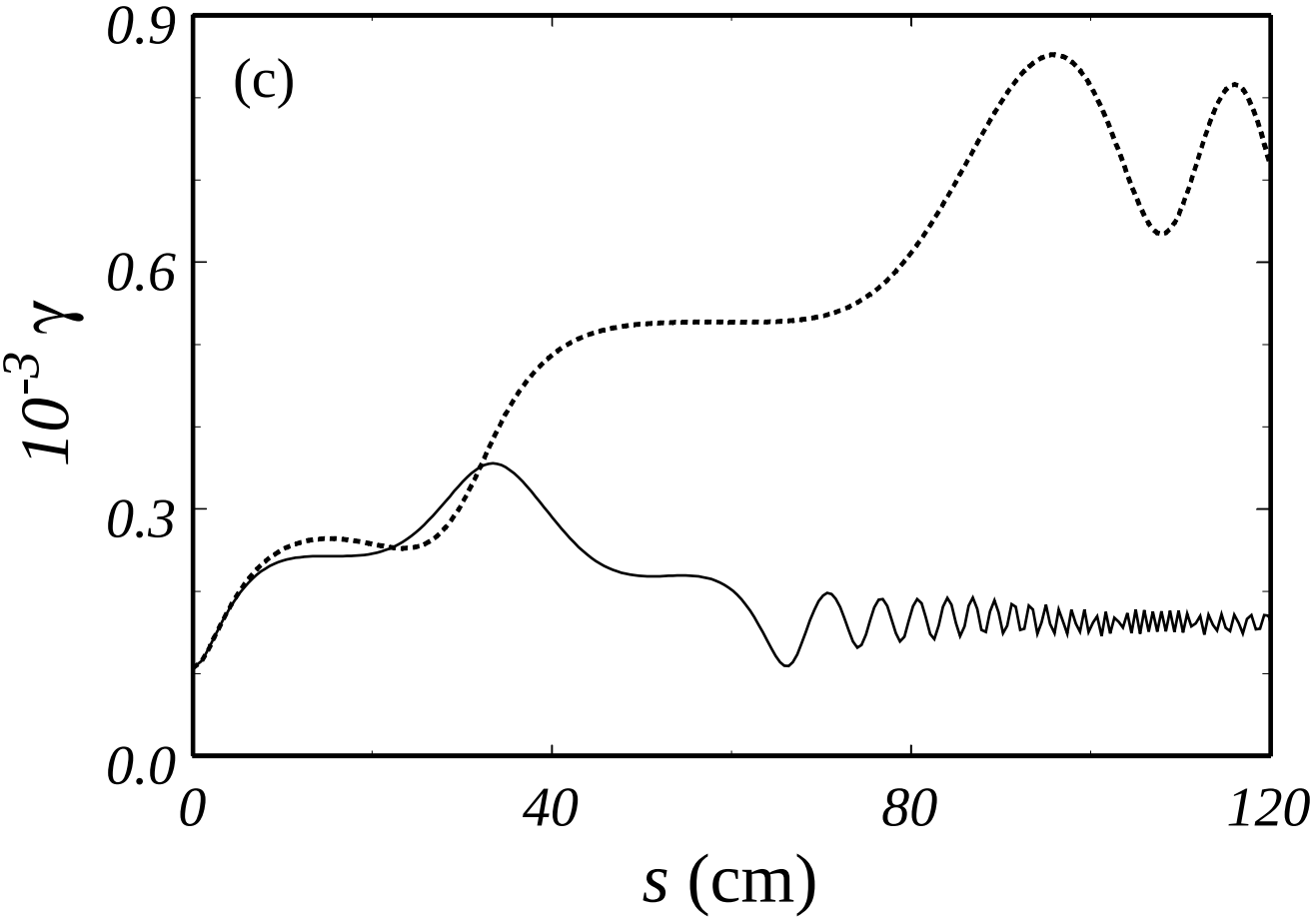

Fig. 2

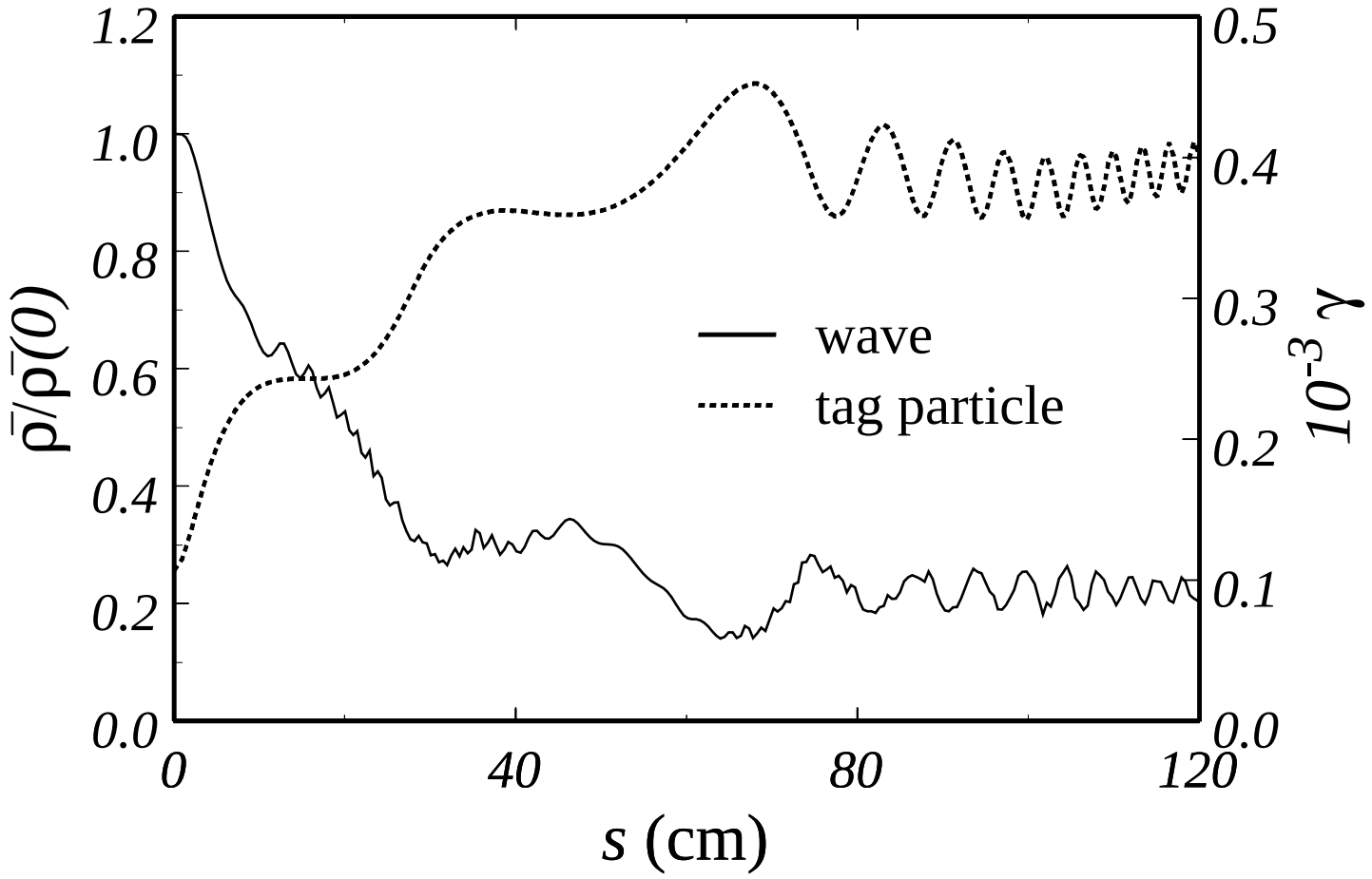
1.2
1.0
0.8
0.6
0.4
0.2
0.0
0.5
0.4
0.3
0.2
0.1
0.0
0
40
80
120
$\bar{\rho}/\bar{\rho}(0)$
$10^{-3}\gamma$
wave
tag particle
s (cm)

Fig. 3